





UNIVERSITY OF HAMBURG

MASTER'S THESIS

---

# A Global Analysis of Mesoscale Eddy Dynamics via a Surface-Signature-Based Tracking Algorithm

---

*Author:*

NIKOLAUS KOOPMANN

*Co-Supervisor:*

PROF. DR. JOHANNA BAEHR

*Supervisor:*

PROF. DR. CARSTEN EDEN

2015/04/14

**TODO: abstract**

will be added last...

# *Contents*

<b>1</b>	<b>Introduction</b>	<b>5</b>
1.1	Theory . . . . .	6
1.2	Important Papers . . . . .	12
1.3	Satellite vs Model Data . . . . .	16
<b>2</b>	<b>Results</b>	<b>19</b>
2.1	MI - 7 day time-step - Aviso . . . . .	22
2.2	MII - 7 day time-step - Aviso . . . . .	24
2.3	MII - 7 day time-step - POP . . . . .	26
2.4	MII - 2 day time-step - POP . . . . .	29
<b>3</b>	<b>Discussion</b>	<b>31</b>
3.1	Lengths of Tracks . . . . .	31
3.2	Scales and the Effect of Downsampling . . . . .	32
3.3	Drift Speeds . . . . .	35
3.4	POP-2day-MII . . . . .	36
<b>Declaration of Authorship</b>		<b>39</b>
<b>Declaration of Authorship</b>		<b>41</b>



# 1

## Introduction

THE MAIN PURPOSE of this study is to investigate the dynamics of geostrophic mesoscale ocean eddies on a global scale. By virtue of the geostrophic character of the scales of concern, such vortices implicate a local upheaval/depression of density surfaces which usually<sup>1</sup> also includes the sea surface.

The resultant *hills* and *valleys* in sea surface anomaly can be resolved by combining multiple satellite-altimetry signals (see fig. 1.1). One motivation of this study is to investigate whether the resolutions in space and time of such altimeter-derived products suffices to successfully track individual eddies over long periods of time and to precisely determine their horizontal extent. The detection/tracking/analyzing procedure of individual eddies is executed globally via an automated parallelized computer-program. To analyze the effects of different time/space-resolutions, a finer-grid SSH-product of a modern ocean-circulation model is subjected to the algorithm as well.

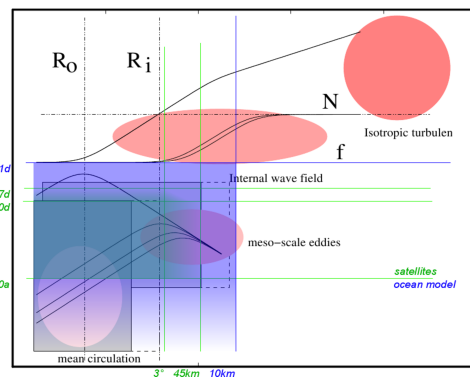


Figure 1.1: Resolutions for model vs satellite.  
Modified version from ?.

DUE to the inherently technical character of the matter, large parts of

<sup>1</sup> As in theory, baroclinic eddies have most of their energy in the first (surface-intensified) baroclinic mode (?).

this text are dedicated to details of the algorithm <sup>2</sup>. Oceanographic results are treated in the [results](#)- and [discussion](#)-chapters. This chapter discusses the physics of mesoscale geostrophic turbulence and introduces a handful of relevant historical papers. Since focus is on horizontal scales, translational speeds and the comparison of results between the Aviso-altimetry product and SSH-data from the POP ocean model, sections generally focus on either of these three topics.

<sup>2</sup> see the ??.

## 1.1 Theory

GEOSTROPHIC turbulence is typically characterized by rather stable, often deep reaching, more or less circular, coherent pressure anomalies that rotate fluid around in a vortex in quasi-geostrophic equilibrium (?). These entities can persist for long periods of time in which they often travel distances on the order of hundreds of kilometers zonally. The fact that baroclinic instability leads to these vortices, instead of cascading to ever smaller scales as would be expected from chaotic turbulence, is a direct consequence of the inverse energy cascade of two-dimensional motion <sup>3</sup> (see ??.) (??). The atmospheric analog are storms and high-pressure systems, yet with much less difference between high- and low-pressure systems due to a smaller centrifugal force *i.e.* smaller Rossby number (Ro). These quasi-geostrophic, mesoscale vortices *i.e.* *eddies* <sup>4</sup>, are immediately visible on SSH-maps (see fig. 1.4). Yet, it is difficult to *define* an eddy in terms of physical variables. The transition from meandering jets or other undeveloped baroclinic turbulence to a coherent vortex is not very sharp. Eddies also sometimes merge or split or collectively form rifts and valleys in SSH. Detecting them on one snapshot automatically via an algorithm is therefore not trivial. Further problems arise when the algorithm is also supposed to track each individual eddy over time. Their sheer abundance at any given point in time inevitably creates ambiguities as to *which is which* between time steps.

### 1.1.1 Detection Methods

- One way to find an eddy in SSH-data is to simply scan for closed contours at different values for  $z$  and then subject found entities to a series of geometrical tests to decide whether the contour qualifies.

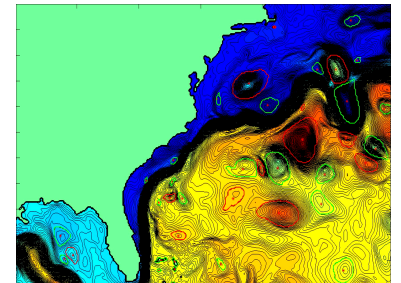


Figure 1.2: Animation snapshot of early test run. Shown is SSH with detected eddies indicated by red and green lines.

<sup>3</sup> For a discussion of this phenomenon see ??

<sup>4</sup> For a discussion of the different types of vortices in the ocean see appendix ??

Only if all criteria are met is an eddy found. This method was first used by ? and is certainly a relatively simple yet very effective method, at least so for satellite data. Therefore, as a starting point, this method will be adopted and should also serve as a general definition of what will be referred to as an *eddy* hereafter.

? set the following threshold criteria for their algorithm:

1. The SSH values of all of the pixels are above (below) a given SSH threshold for anticyclonic (cyclonic) eddies.
  2. There are at least  $[threshold]$  pixels and fewer than  $[threshold]$  pixels comprising the connected region.
  3. There is at least one local maximum (minimum) of SSH for anticyclonic (cyclonic) eddies.
  4. The amplitude of the eddy is at least  $[threshold]$ .
  5. The distance between any pair of points within the connected region must be less than  $[threshold]$ .
- Another frequently used method to define an eddy makes use of the 2d deformation tensor  $\nabla \mathbf{u}$ .

$$\det(\lambda \mathbf{I} - \nabla \mathbf{u}) = 0 \quad (1.1)$$

The Sign of its squared eigenvalues indicates whether the flow-field has parabolic, vorticity dominated character, or whether deformation dominates, giving hyperbolic character. Expanding equation (1.1) yields

$$\lambda^2 - \lambda(v_y + u_x) + u_x v_y - u_y v_x = 0 \quad (1.2)$$

Assuming horizontal velocities to be much larger than vertical *i.e.* applying the small aspect-ratio assumption (?), the motion becomes 2-dimensional and the continuity equation reduces to  $u_x = -v_y$ . Hence

$$\lambda^2 = O_w/4 = u_x^2 + u_y v_x \quad (1.3)$$

This is called the Okubo-Weiss-Parameter <sup>5</sup>  $O_w$  (?). Its meaning is

<sup>5</sup> see also ??

further elucidated by interpreting equation (1.3) as

$$\begin{aligned}
 O_w &= s_n^2 + s_s^2 - \omega^2 + \nabla \cdot \mathbf{u} \\
 &= (u_x - v_y)^2 + (v_x + u_y)^2 - (v_x - u_y)^2 + (u_x + v_y)^2 \\
 &= (u_x^2 - 2u_xv_y + v_y^2) + (v_x^2 + 2v_xu_y + u_y^2) - (v_x^2 - 2v_xu_y + u_y^2) + 0 \\
 &= (u_x^2 - 2u_xv_y + v_y^2) + 4v_xu_y \\
 &= (u_x^2 + 2u_x^2 + u_x^2) + 4v_xu_y \\
 &= 4u_x^2 + 4v_xu_y
 \end{aligned} \tag{1.4}$$

where  $s_{n/s}$  are the normal respective shear components of strain. Its sign thus describes the field's tendency for either vorticity- or shear-dominated motion (?). An area of large negative values of  $O_w$  indicates high enstrophy density compared to gradients of kinetic energy <sup>6</sup>, thus indicating little friction paired with high momentum *i.e.* a vorticity dominated field as would be found in a coherent, angular-momentum-conserving entity. Positive values on the other hand indicate motion dominated by deformation as *e.g.* in-between two vortices of opposite sign. The fourth term, which is irrelevant here, represents divergence and can here be interpreted as negative *vortex stretching* (*e.g.* bathtub sink).

<sup>6</sup>

As useful as this parameter seems, it turns out that using it to identify eddies is often not practical. ? name 3 major drawbacks:

- No single threshold value for  $O_w$  is optimal for the entire World Ocean. Setting the threshold too high can result in failure to identify small eddies, while a threshold that is too low can lead to a definition of eddies with unrealistically large areas that may encompass multiple vortices, sometimes with opposite polarities.
- $O_w$  is highly susceptible to noise in the SSH field. Especially when velocities are calculated from geostrophy, the sea surface has effectively been differentiated twice and then squared, exacerbating small incontinuities in the data.
- The third problem with the W-based method is that the interiors of eddies defined by closed contours of  $W$  do not generally coincide with closed contours of SSH. The misregistration of the two fields is often quite substantial.

In summary, the  $O_w$ -method critically hinges on the necessary assumption of a smooth, purely geostrophic SSH topography

and is therefor inferior to the approach of scanning for closed SSH-contours directly (as was done so by ?) (see also ?).

### 1.1.2 Eddy Drift Speeds

INTUITIVELY any translative motion of a vortex should stem from an asymmetry of forces as in an imperfectly balanced gyroscope wobbling around and translating across a table. The main effects that cause a quasi-geostrophic ocean eddy to translate laterally can be explained rel. easy heuristically:

#### Drift Speed 1.1.2.1: Lateral Density Gradient

Consider a mean layer-thickness gradient  $\frac{\partial h}{\partial x} > 0$  somewhere in the high northern latitudes and a geostrophic, positive density anomaly within that layer. In other words, a high-pressure vortex or an anti-cyclonic eddy with length scale  $L \approx L_R$ . Next consider a parcel of water adjacent to the eddy's northern flank of initially zero relative vorticity that is being entrained by the eddy. As the clockwise rotating eddy advects the parcel towards its eastern side, the water-column comprising said fluid will be stretched vertically as it is advected towards larger depths. In order to maintain total vorticity a small new relative-vorticity term is introduced via term  $C$  in equation (??). Since the vorticity budget is dominated by the planetary component, this new term has sign of  $f$  i.e. **positive**. The opposite effect holds for a parcel advected towards the western side. Then, vortex *squeezing* leads to a new **negative** relative-vorticity term. Hence water masses on both sides of the thickness gradient acquire rotation that slowly pushes the eddy in the direction  $-f \times \frac{\partial h}{\partial x}$  (in this case south). Note that since vorticity is dominated by the planetary component, the rotational sense of the eddy is irrelevant here. I.e. water columns stretched [squeezed], will always lead to new  $\omega$  with sign of  $f$   $[-f]$ .

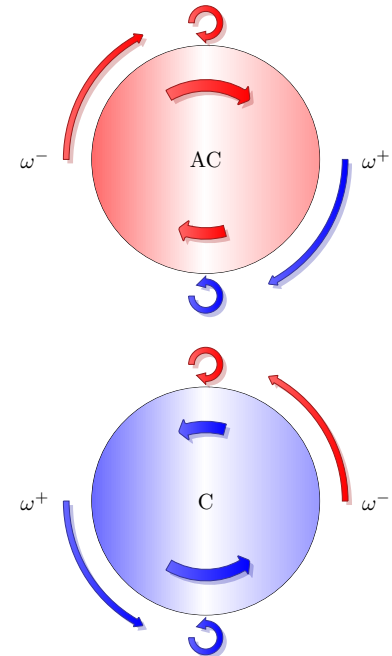


Figure 1.3: Bottom [Top]: Northern hemisphere [anti]cyclone. Blue [red] color indicates presence/production of positive [negative] relative vorticity. Advection of adjacent water masses leads to a westward drift, irrespective of the eddy's sign (see drift speed box 1.1.2.2). Inside, the discrepancy in swirl strength between north and south requires another (smaller) zonal drift term, which is eastward [westward] for [anti]cyclones.

#### Drift Speed 1.1.2.2: Planetary Lift

Assume now that  $\beta L$  be comparable or larger even than  $f + \omega$  from the previous example. Then, independent of layer-thickness, all fluid adjacent to the eddy on its northern and southern flanks will be transported meridionally, thereby be tilted with respect to  $\Omega$  and hence acquire relative vorticity to compensate. All fluid

transported north [south] will balance the increase in planetary vorticity with a decrease [increase] in relative vorticity. This is again independent of the eddy's sense and in this case also independent of hemisphere since  $\frac{\partial f}{\partial y} = \beta > 0$  for all latitudes. The result is that small negative vortices to the northern and small positive vortices to the southern flank of eddies will push them west.

#### Drift Speed 1.1.2.3: Eddy-Internal $\beta$ -Effect

In the later case clearly particles within the vortex undergo a change in planetary vorticity as well. Or from a different point of view, since  $U \sim \nabla p/f$ , and noting that the pressure gradient is the driving force here and hence fix at first approximation, particles drifting north will decelerate and those drifting south will accelerate. In order to maintain mass continuity, the center of volume will be shifted west for an anti-cyclone and east for a cyclone. Another way to look at it is to note that the only way for the discrepancy in Coriolis acceleration north and south, whilst maintaining constant eddy-relative particle speed, is to superimpose a zonal drift velocity so that net particle velocities achieve symmetric Coriolis acceleration.

### 1.1.3 Eddy Horizontal Scales

THIS section discusses the motivation for exact determinations of eddy scales. That is, their horizontal extent *i.e.* their diameter or *wavelength*.

JUST like the eddy itself, its scale is rather vague and difficult to define. What physical parameter defines the outer edge of a seamless, smooth vortex? If the eddy is detected as done by ?, *i.e.* closed contours of SSH, the interior of which fulfilling certain criteria, the measured perimeter may jump considerably from one time step to the next. An incremental difference in the choice of  $z$  might translate to a perimeter outlining twice the difference in area, especially when SSH gradients are small.

Another possibility is to define an amplitude first, then assume a certain shape *e.g.* Gaussian, and then infer the radius indirectly. The

obvious problem with this approach would be to properly define the amplitude.

The most physically sound method would have to be one depending on the eddy's most defining physical variable that is unambiguously determinable from SSH: the geostrophic velocities. ?, as with everything else, tried all methods but conclude that the later is the most adequate one <sup>7</sup>.

CONSTRUED as an integral length scale of turbulence *i.e.* as the distance at which the auto-correlation of particles reaches zero (??), the eddy-scale turns out to be of fundamental relevance for attempts to parametrize geostrophic turbulence.

GENREAL CIRCULATION MODELS ( $\mathcal{O}(10^2)$  km) as they are used in *e.g.* climate forecasts are too coarse to resolve mesoscale ( $\mathcal{O}(10^1)$  km) turbulence (?????) . Even if the Von-Neumann-condition was ignored and a refinement was desired horizontally only, a leap of one order of magnitude would effect an increase in calculation time <sup>8</sup> of factor  $x = 100$ . The effects of the nonlinear terms therefore have to be somehow articulated in an integral sense for the large grid-boxes in the model (??????). A common approach is to assume that eddy kinetic energy  $\overline{u'u'}$  and eddy potential energy  $\overline{w'p'}$ , akin to diffusive processes<sup>9</sup> , were proportional to the gradient of  $\bar{u}$  respective  $\bar{b}$  (down-gradient-parametrization <sup>10</sup>) (??), which leads to the problem of finding expressions for the *turbulent diffusivities* *i.e.* the rate at which gradients are diffused by turbulence. This parameter is by no means constant, instead it can span several orders of magnitude, itself depending on the strength of turbulence-relevant gradients, and sometimes even assuming negative values (?). Precise knowledge of the integral length scale and the physics that set it is hence vital for attempts to analyze and set values for eddy diffusivites and turbulence parameterizations in general.

**TODO:** [...] i took out section on eddy diffusivities

## 1.2 Important Papers

THE following discusses a handful of selected historical papers that are concerned with either the theory of mesoscale eddies or with the detection/tracking of eddies from SSH data.

<sup>7</sup> See ??

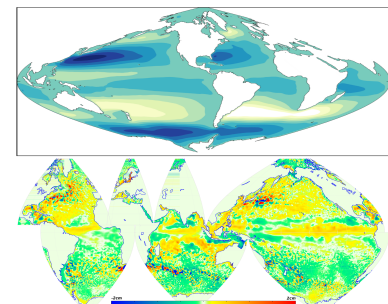


Figure 1.4: top: Stommel's equation  $F_{bottom} - F_{surface} = -V\beta$  with constant eddy viscosity. bottom: POP eddy-resolving model snapshot with SSH mean of one year subtracted.

<sup>8</sup> With the Moore's-Law-type exponential growth in FLOP/S of the last 22 years for supercomputers ( $\lg(x) \sim 3/11a$ ) a factor 100 interestingly translates to only  $a = 22/3 \approx 7$  years...

<sup>9</sup> In analogy to Fick's first law of diffusion.

<sup>10</sup> *i.e.* Reynolds averaging

### 1.2.1 Waves and Turbulence on a $\beta$ -Plane<sup>11</sup>

Rhines investigated the effect of the  $\beta$ -plane on the inverse energy cascade of quasi-2-dimensional atmospheric and oceanic turbulence. At constant  $f$ , energy should be cascaded to ever-larger scales until halted by the scale of the domain. This is clearly not the case, as no storm has ever grown to global scale. The presence of a meridional restoring force creates a critical scale beyond which the *turbulent migration of the dominant scale nearly ceases* .... Rossby waves are excited which would in theory eventually give way to alternating zonal jets of width  $\frac{U}{\beta}$ . This scale was later coined the Rhines Scale  $L_\beta$ .

### 1.2.2 Westward Motion of Mesoscale Eddies<sup>12</sup>

? already noted that the  $\beta$ -effect causes a mass-imbalance in planetary vortices that, if not met by an asymmetry in shape must lead to westward propagation.

? derived that the  $\beta$ -effect results in a net meridional force on the integrated mass of the vortex, which in balance with the Coriolis acceleration shoves cyclones eastward and anti-cyclones westward. They also explained how displaced water outside the eddy's perimeter causes a much stronger westward component, with the result that all eddies propagate westward irrespective of rotational sense.

The westward drift was also derived in various forms by e.g. ??.

THE paper by ? is particularly helpful to understand where the two components of westward drift come from. By scaling the terms in the one-layer primitive equations by their respective dimensionless numbers, integrating the interface-displacement caused by the eddy over the eddy's domain and applying mass continuity they derive for the location  $(X, Y)$  of an eddy's centroid<sup>13</sup>:

$$\Pi X_{tt} - Y_t = L_R^1 T \beta \langle yv \rangle + L \frac{\beta}{f} \langle y\eta v \rangle \quad (1.5)$$

$$\Pi Y_{tt} - X_t = -L_R^1 T \beta \langle yu \rangle - L \frac{\beta}{f} \langle y\eta u \rangle \quad (1.6)$$

where  $\Pi = 1/f_0 T$ .

Hence, independent of balance of forces the eddy's center of mass describes inertial oscillations<sup>14</sup> on the  $f$ -plane, even in the absence of  $\beta$ . Using geostrophic values for  $u$  and returning to dimensional

<sup>13</sup>  $\langle \rangle \equiv \frac{1}{A} \int_A dA$

<sup>14</sup> compare to harmonic oscillator

variables equation (1.5) can be cast into:

$$\begin{aligned}\frac{\partial X}{\partial t} &= \frac{\beta g'}{f_0^2} \frac{\int_A H\eta \, dA + \int_A \eta^2/2 \, dA}{\int_A \eta \, dA} \\ &= \beta \left( \frac{NH}{f_0} \right)^2 + \frac{\int_A \eta^2/2 \, dA}{\int_A \eta \, dA} \\ &= \frac{\partial \omega_{long}}{\partial k} + u_{internal}\end{aligned}\quad (1.7)$$

THE first term of the RHS of equation (1.7) represents the *planetary lift*<sup>15</sup>, which is identical to the zonal group velocity of long Rossby waves (?). The second term  $u_{internal}$  represents the *eddy-internal  $\beta$ -effect* (see drift speed box 1.1.2.3)<sup>16</sup>. Note that the first term is always westwards, while the second has sign of  $-\eta$ , i.e. westward for anti-cyclones and eastward for cyclones and that the first is always much larger than the second.

<sup>15</sup> see drift speed box 1.1.2.2 from section 1.1.2

<sup>16</sup> see also ??

### 1.2.3 Early Altimeter Data

THE advent of satellite altimetry, which Walter Munk called *the most successful ocean experiment of all time* (?), finally allowed for global-scale experimental investigations of oceanic planetary phenomena on long time- and spatial scales. Among others, ??? were the first to use satellite-data to present evidence for the existence of Rossby waves and their westward-migration in accord with theory. Surprisingly all of the observations found the phase speeds to be 1 to 1.5 times larger than what theory predicted. Several theories to explain the discrepancy were presented. E.g. ? argued that the discrepancy was caused by mode-2-east-west-mean-flow velocities. Interestingly it appears that hitherto, the relevant altimeter signal was mainly associated with linear waves. Non-linearities are rarely mentioned in the papers of those years. Probably simply due to the fact that the turbulent character of much of the mesoscale variability was still obscured by the poor resolution of the first altimeter products.

### 1.2.4 SSH Altimeter Data<sup>17</sup>

<sup>17</sup>; and

From the beginning of satellite altimetry ? have invested tremendous effort to thoroughly analyze the data in terms of Rossby waves and geostrophic turbulence. At the time of the ? paper only 3 years of

Topex/Poseidon data alone had been available, which led them to interpret the data mainly in terms of Rossby waves. Once the merged Aviso T/P and ERS 1/2 (?) was released 7 years later, ? presented a new analysis that was based on an automated eddy-tracking algorithm using the geostrophic Okubo-Weiss parameter<sup>18,19</sup>. For the first time satellite data was resolved sufficiently fine to unveil the dominance of *blobby structures rather than latitudinally  $\beta$ -refracted continuous crests and troughs* that had hitherto been assumed to characterize the large-scale SSH topography. They presented results of a refined algorithm in their ? paper, in which they abandoned the Okubo-Weiss concept and instead identified eddies via closed contours of SSH itself<sup>20</sup>. The improved algorithm and longer data record now allowed them to separate the non-linear eddy activity from the larger-scale Rossby waves. They find that the vast majority of extra-tropical westward propagating SSH variability does indeed consist of coherent, isolated, non-linear, mesoscale eddies that propagate about 25% slower<sup>21</sup> than the linear waves. Apart from this though they find little evidence for any dispersion in the signal, neither do they find evidence for significant meridional propagation, as should be found for Rossby waves (? , chapter 8.2.1). In agreement with ?, they find this eddy-dominated regime to fade towards the equator, giving way to the characteristic Rossby wave profile. Almost all of their eddies propagate westwards. Those eddies that are advected eastwards by e.g. the ACC show significantly shorter life-times than those that are not. For more detail on their results and a discussion of the limitations of eddy-tracking via satellites (see section 1.3).

<sup>18</sup> see section 1.1.1

<sup>19</sup> see Derivation ??

<sup>20</sup> note that geostrophic  $O_W$  is a second derivative of SSH and thus exacerbates noise in the SSH data.

<sup>21</sup> pointing to dispersion.

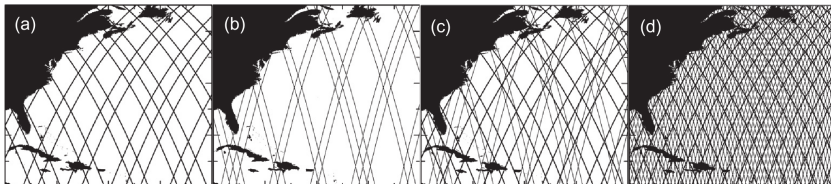
**TODO:** i took out...

- ????????????????

### 1.3 Satellite vs Model Data

THE latest Aviso SSH data from satellites features impressive accuracy, constancy and resolutions in both space and time. This is achieved by collecting all of the data from all of the altimeter-equipped satellites available at any given moment for any given coordinate. This conglomerate of highly inhomogeneous data is then subjected to state-of-the-art interpolation methods to produce a spatially and temporally coherent product. One satellite alone is not sufficient to adequately resolve mesoscale variability globally.

E.g. the Topex/Poseidon satellite had a ground repeat track orbit of 10 days and circled the earth in 112 minutes or  $\approx 13$  times a day with a swath width of 5 km. Hence it drew  $\sim 26$  5-km-wide stripes onto the globe every day. The orbit's precession is such that this pattern is then repeated after 10 days, which means that at the equator only  $10 \times 26 \times 5 = 1300$  km of the  $2\pi \times 6371 = 40\,000$  km get covered, *i.e.* 3.25%. At every 10 d time-step, on average, effectively  $(40000 - 1300)/26 = 1490$  km are left blank in-between swaths on the equator. This is why, no matter how fine the resolution within the swath at one moment in time may be, the spatial resolution is so coarse. The merged ERS-1/Topex-data as used by ? has a time step of 7 days. Assuming eddy drift speeds of  $u_e = \mathcal{O}(10^{-1})$  m/s implies a distance traveled per time step of  $L_{\delta t} \approx 60$  km. ? estimate their effective spatial resolution as  $\delta x \approx 40$  km. Eddies of smaller scale are not resolved.



TRACKING a single eddy from one time-step to the next is complicated

	POP	merged T/P - ERS-1
dx	7km 11km	1/3° ( $\approx 40$ km after filtering)
dt	1d	7d
$\log_{10} 2$ filter cutoff	-	2° by 2°
z-levels	4 <sup>2</sup>	1
variables	SSH, S, T, u/v/w, tracers etc	SSH
pot. interpo- lation artifacts	-	yes
reality	no	yes

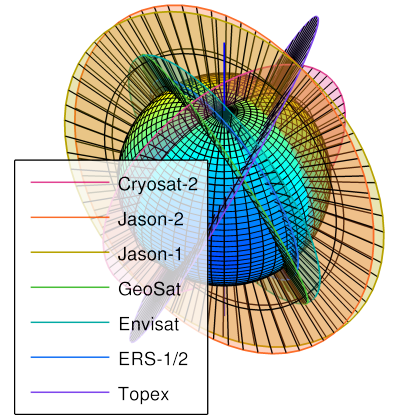


Figure 1.5: The ground track patterns for the 10-day repeat orbit of T/P and its successors Jason-1 and Jason-2 (thick lines) and the 35-day repeat orbit of ERS-1 and its successors ERS-2 and Envisat (thin lines). (a) The ground tracks of the 10-day orbit during a representative 7-day period; (b) The ground tracks of the 35-day orbit during the same representative 7-day period; (c) The combined ground tracks of the 10-day orbit and the 35-day orbit during the 7-day period; and (d) The combined ground tracks of the 10-day orbit and the 35-day orbit during the full 35 days of the 35-day orbit. (sic) (?)

by the sheer abundance of eddies at any given point in time and the fact that eddy activity is usually concentrated into regions of strong geostrophic turbulence. The ambiguities in matching the eddies from the old time-step to those of the new one might cause aliasing effects in the final statistics.

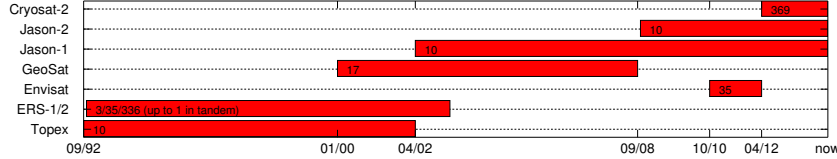


Figure 1.6: Length of mission. Numbers are orbit-period in days.

THE translational speeds <sup>22</sup> of eddies are not really the problem here, as they usually drift slow enough to not cover more than 1 grid node per 7 day time step. The issue are those areas where eddies are born, die and merge. According to ?, instabilities within the ACC grow at rates of up to  $1/(2\text{days})$ , which means that at one time-step up to 3 eddies have emerged and equally many died for every eddy identified within such region. The ground-repeat-frequency of a satellite can of course not be set arbitrarily. Especially when the satellite is desired to cover as far north and south as possible, whilst still being subjected to just the right torque from the earth's variable gravitational field to precess at preferably a sun-synchronous frequency *i.e.*  $360^\circ/\text{year}$  (?). Neither can the satellite's altitude be chosen arbitrarily. If too low, the oblateness of the earth creates too much eccentricity in the orbit that can no longer be *frozen* <sup>23</sup>. Another problem could be potential inhomogeneity in the merged data in time dimension, since data of old and current missions are lumped together into one product. This is why ? opted against the finest resolution available and instead went for a product that had the most satellites merged in unison for the longest period of time.

<sup>22</sup>  $\mathcal{O}(10^1)\text{km/day}$

<sup>23</sup> minimizing undulating signals in altitude by choosing the right initial values (?)

THE surface velocities inferred from altimetry are the geostrophic components only, which should suffice to *e.g.* determine the non-linearity and kinetic energy of an eddy for almost all regions, but less so for *e.g.* the western boundary currents.

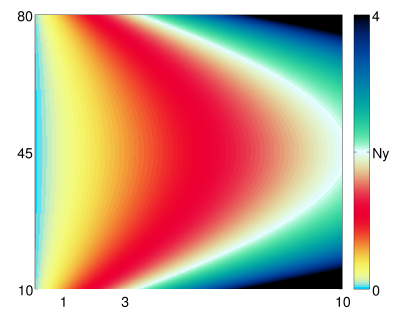


Figure 1.7:  $\xi(\phi, \mu)$ .  $Ny \equiv 2$  *i.e.* the Nyquist frequency.

**Box 1: Horizontal Resolution**

Assume  $Bu = 1$ , so that  $L = NH/f$  and  $NH = a/10d$  (corresponds to  $L(\phi = 30^\circ) = 100\text{km}$ ), a model resolution of  $1^\circ/\mu$  and that the eddy diameter was twice the Rossby radius. Then, how many grid notes  $\xi$  fit into one eddy as a function of latitude?

$$\begin{aligned}\xi \frac{a \cos \phi}{\mu} &= \frac{2NH}{f} = \frac{2NH1d}{4\pi \sin(\phi)} \\ \xi &= \frac{2\mu}{10 \sin(2\phi)}\end{aligned}\tag{1.8}$$

In this flat-bottom, constant  $\rho_z$ , Mercator-gridded model the worst eddy-resolution is interestingly at mid-latitude (see fig. 1.7).

THE finer resolution of the POP data in space and time should certainly yield more precise results. It must be kept in mind though that by using the model data, what one analyses is of course just that - a *model*. Baroclinic geostrophic space/time scales depend crucially on e.g. the vertical density structure (see section 1.2.2, ?), which is resolved only poorly in the model. A useful comparison among satellite/model results should hence be tricky.

## 2

# Results

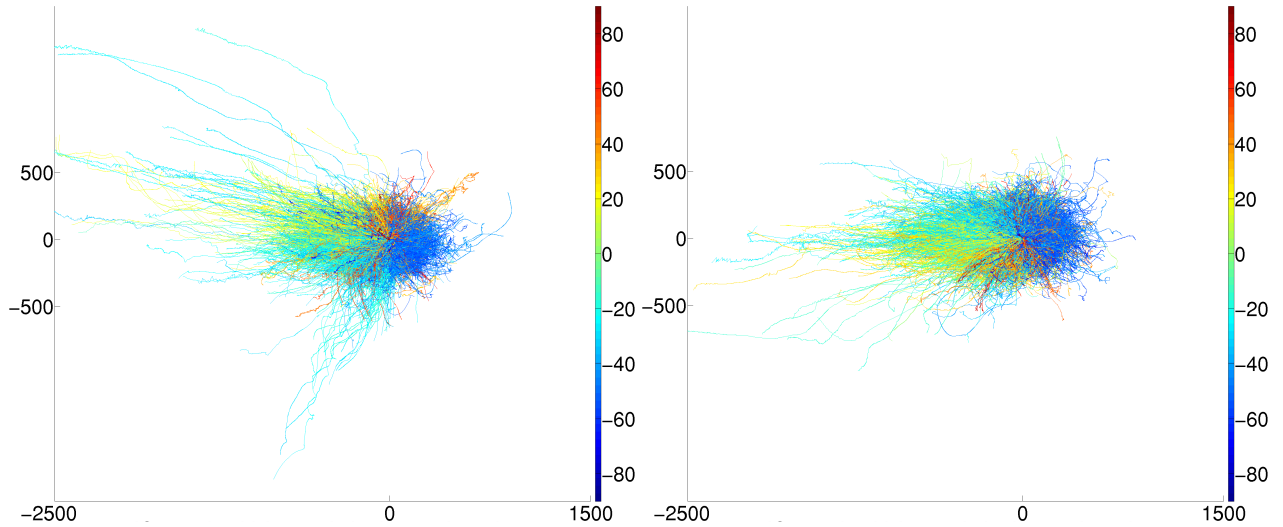


Figure 2.1: Baseline-shifted tracks. Left: anticyclones. Right: cyclones. Color represents *birth-latitude*. Thickness (hardly noticeable) represents IQ. Data is from a predecessor run to POP-7day MII .

<sup>1</sup> depending on the number of cpu's and their frequencies.

<sup>2</sup> see section 3.1

EVEN though all of the computer program's bottle-necks are parallelized in SPMD, an application to more than a decade of high-resolution SSH data still requires patience (say  $\mathcal{O}(10^1)$  -  $\mathcal{O}(10^2)$  days<sup>1</sup>). The most time-consuming of steps is the numerically arduous part of subjecting each of the vast number of found contours<sup>2</sup> to the filtering procedure as described in ?? . The total number of final analyses was hence limited and it was therefor critical to carefully choose which method/parameters to use in order to maximize the deducible insights from the results. For best comparability of the results with each other it was decided to agree on one complete set of parameters

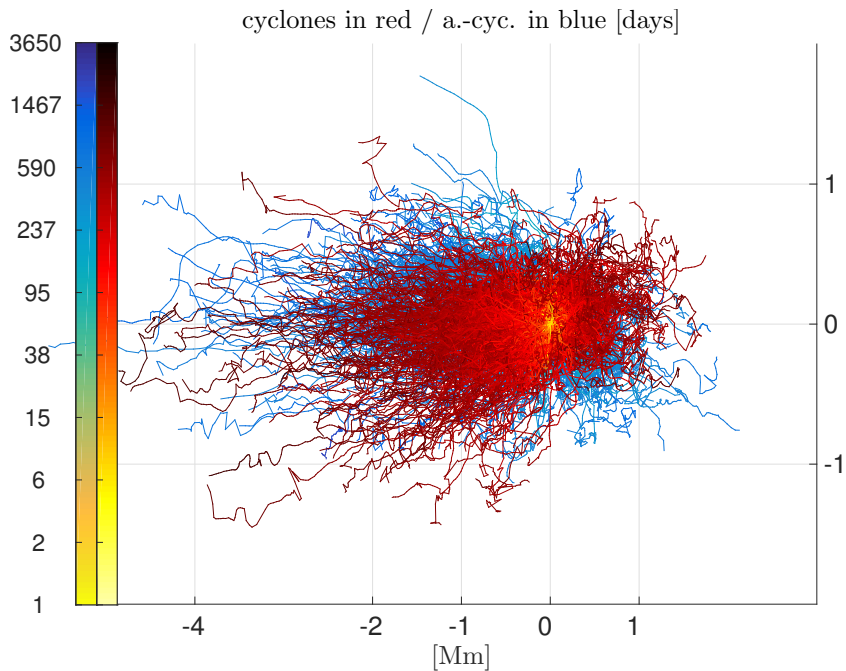


Figure 2.2: Aviso-MI : Baseline-shifted old ( $> 500$  d) tracks.

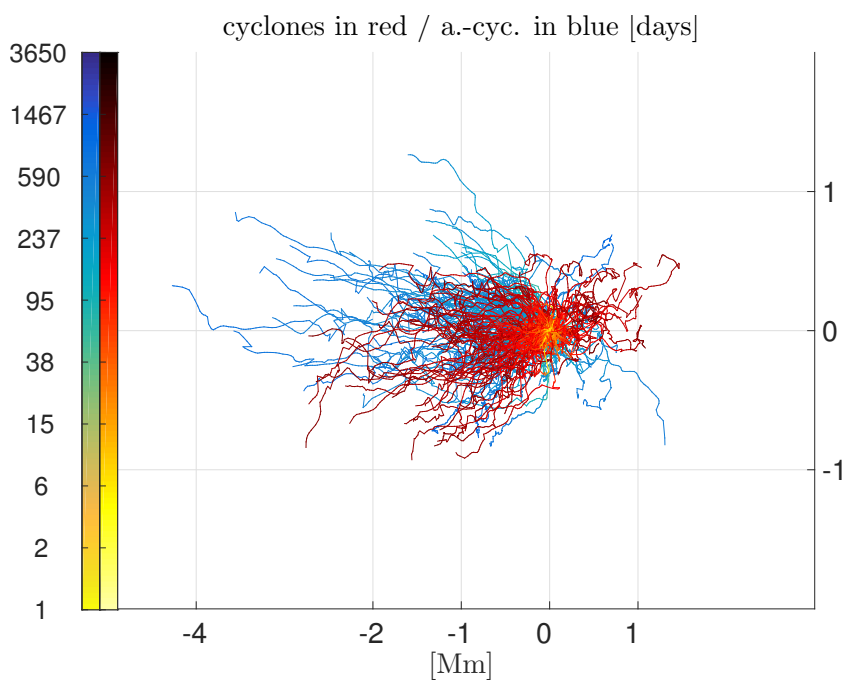


Figure 2.3: Aviso-MII : (same as fig. 2.2)

as a basis (chapter 2), which would then be altered at key parameters.

- The first run is an attempt to reproduce the results from ?. The SSH-data for this run is therefore that of the Aviso product. This method will be called **MI**.
- The second run (**MII**) is equivalent, except that this time the alternative IQ-based shape filtering method as described in ?? and the slightly different tracking-filter as described in ?? are used. **MII** is then fed with 7-day time-step POP data as well.
- To investigate what role spatial resolution plays, the POP data was remapped to that of the Aviso data and fed to the **MI** method.
- Finally, to investigate the effects of resolution in time, an **MII**-2-day-time-step run over POP data was executed. For its results and discussion see section 3.2.
- **TODO:** `popTwoII`
- Start and end dates were fix for all runs as the intersection of availability of both data sets.

#### Box 2: Method **MI**

The concepts used in this method are mostly based on the description of the algorithm described by ? and all parameters are set accordingly. Basically **MI** is a modification of **MII** (which was completed first), with the aim to try to recreate the results from ?. It differs from **MII** in the following:

- **detection**

As mentioned in ??, the approach by ? is to avoid overly elongated objects by demanding:

- high latitudes

The maximum distance between any vertices of the contour must not be larger than  $400\text{km}$  for  $|\phi| > 25^\circ$ .

- low latitudes

The  $400\text{km}$ -threshold increases linearly towards the equator to  $1200\text{km}$ .

- **tracking**

time frame	1994/01/05 - 2006/12/27
scope	80°S to 80°N / full zonal.
Aviso geometry	641x1440 true Mercator
POP geometry	2400x3600 mixed proj.
contour step	0.01 m
<b>thresholds</b>	
max $\sigma/L_R^1$	4
min $L_R^1$	$20 \times 10^3$ m
min IQ	0.55
min number of data comprising found contour	8
max(abs(Rossby phase speed))	$1 \text{ m s}^{-1}$
min amplitude	0.01 m

Table 2.1: Fix parameters for all runs.

The other minor difference to [MII](#) is in the way the tracking algorithm flags eddy-pairs between time-steps as sufficiently similar to be considered successful tracking-candidates (see [??](#)). In this method an eddy B from time-step  $k + 1$  is considered as a potential manifestations of an eddy A from time-step  $k$  as long as both - the ratio of amplitudes (with regard to the mean of SSH within the found contour) and the ratio of areas (interpolated versions as discussed in TODO ref) fall within a lower and and an upper bound.

### Box 3: Method [MII](#)

The purpose of this variant is basically to test the conceptually different approach of using the [isoperimetric quotient](#) to judge the shape of found contour-rings as sufficiently eddy-*typical*. It also uses a slightly different tracking algorithm.

- **detection**

The IQ-method. See [??](#) and figs. [3.2](#) and [3.3](#) and [??](#).

- **tracking**

Conceptually similar to [MI](#), it is again vertical and horizontal scales that are compared between time-steps. Preferring a single threshold-value over one upper and one lower bound, a parameter  $\xi$  was introduced that is the maximum of the two values resulting from the two ratios of amplitude respective  $\sigma$ , where either ratio is -if larger- its reciprocal in order to equally weight a decrease or an increase in respective parameter. In other words:  $\xi = \max([\exp|\log R_\alpha|; \exp|\log R_\sigma|])$ , where  $R$  are the ratios.

## 2.1 MI - 7 day time-step - Aviso

THE RESULTS from the [MI](#)-method are special in that they feature many long-lived eddies (see figs. [2.2](#), [2.4](#) and [2.5](#)), some of which travelled more than 4000 km west. Tracks were recorded throughout the entire world ocean with the only exceptions being an approximately 20°-wide stripe along the equator. The highest count of unique eddies

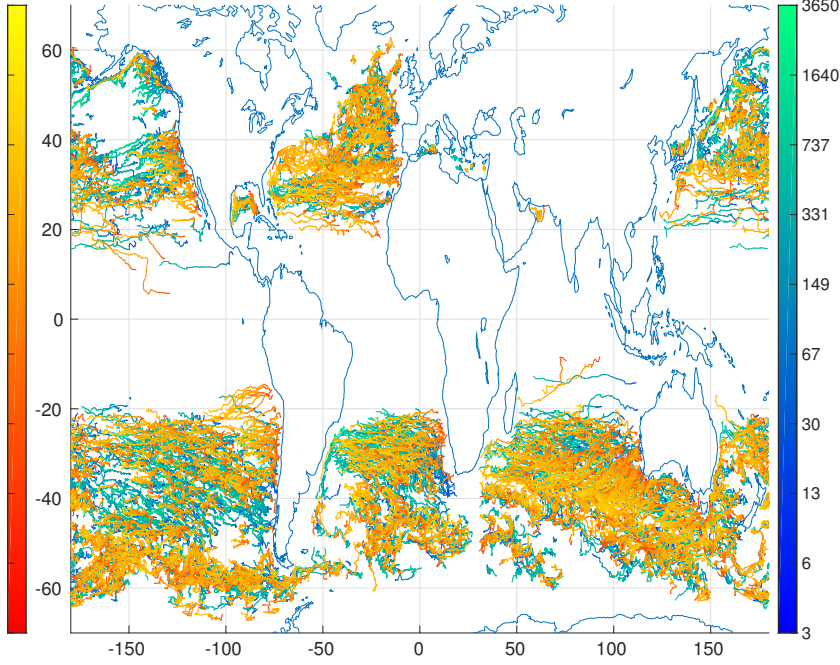


Figure 2.4: MI: Cyclones in red. Tracks younger than 1a omitted for clarity.

is along the Antarctic Circumpolar Current<sup>3</sup> with counts of more than 60 individual eddy-visits per  $1^\circ \times 1^\circ$ -cell. Further eddy-rich regions are the western North-Atlantic throughout the Gulf-Stream and North-Atlantic Current, *Mozambique eddies* (?) at  $20^\circ$  South along the Mozambique coast, along the Agulhas Current and south of the Cup of Good Hope at  $\sim 40^\circ$ , along the coasts of Brazil, Chile and all along the Eastern, Southern and Western coasts of Australia (see fig. 2.7). Eddies appear and disappear throughout the world ocean. For long-lived solid eddies there is a tendency to emerge along western coasts (see ??).

<sup>3</sup> abbreviated ACC from here on.

THE SCALE  $\sigma$  of tracked eddies is similar to that in ?, yet generally smaller in high latitudes and slightly larger in low latitudes (see ??). It is larger than the first-mode baroclinic Rossby Radius by a factor of at least 2 and its meridional profile appears to be separable into two different regimes; one apparently linear profile in low latitudes and a steeper one equator-wards of  $\sim |15^\circ|$ . Regionally, locations of high mesoscale activity appear to correlate with smaller eddy-scales (see ??).

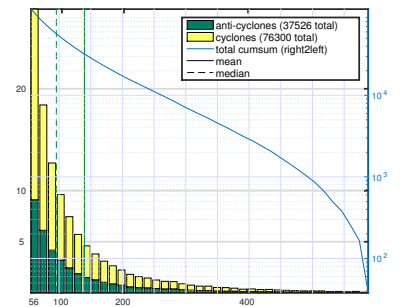


Figure 2.5: Aviso-MI : Final age distribution. x-axis: [days], Left y-axis: [1000]

THE EASTWARD ZONAL DRIFT SPEEDS are slightly slower than the first-mode baroclinic Rossby-Wave phase-speed and agree well with the results from ?. Propagation is generally west-wards except for regions of sufficiently strong eastward advection as in the ACC and North Atlantic Current (see ???).

places of birth and death. size indicates final age.

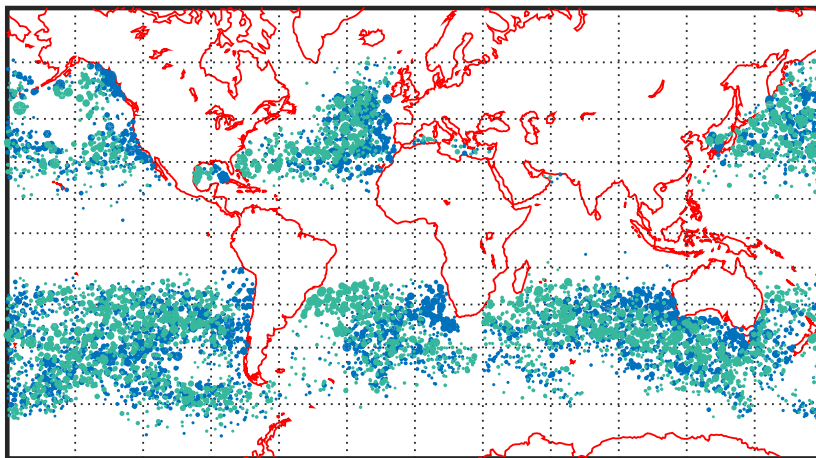


Figure 2.6: Aviso-MI : Births are in blue and deaths in green. Size of dots scales to age squared. Only showing tracks older than one year.

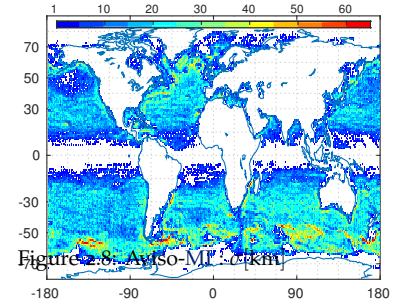
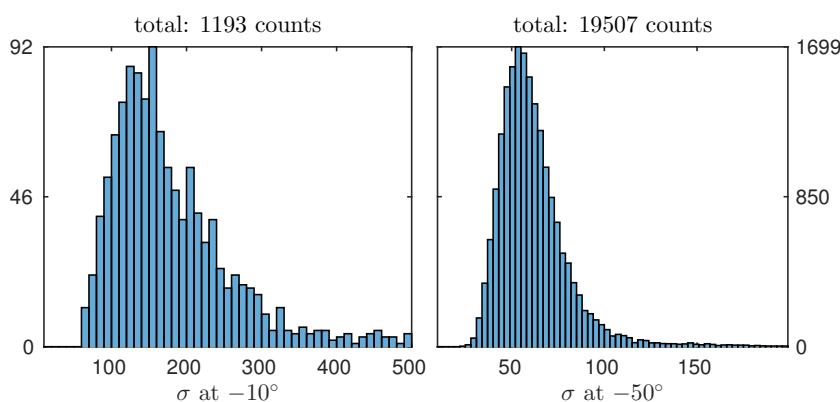


Figure 2.7: Aviso-MI : Total count of individual eddies per 1 degree square.

## 2.2 MII - 7 day time-step - Aviso

THE IQ-based method results in approximately the same total amount of tracks as the MI-method used in section 2.1 (see figs. 2.5 and 2.10).

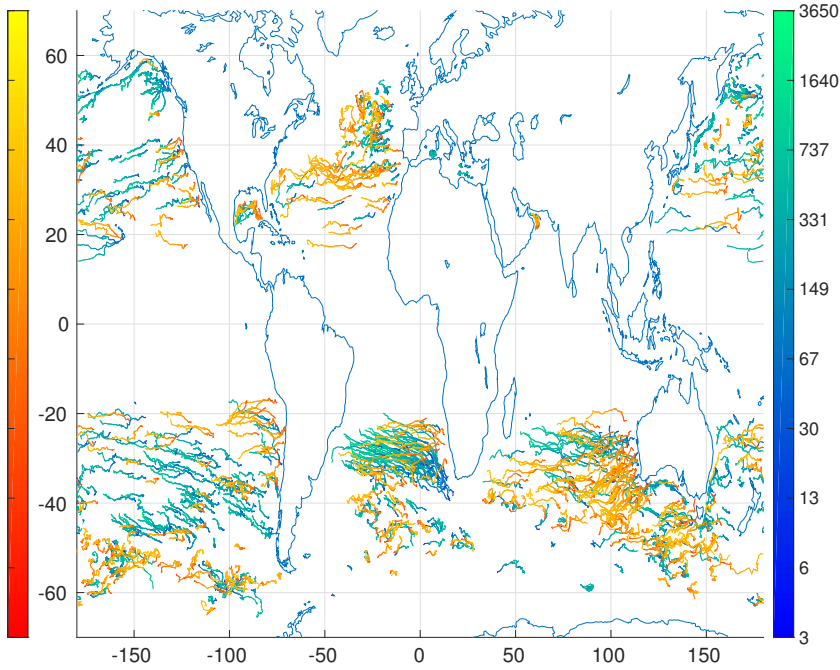


Figure 2.9: MII: (see fig. 2.4)

The difference is that tracks here are generally much shorter, meaning that less eddies are detected at any given point in time. The scale  $\sigma$  is now smaller than that from ? for all latitudes in zonal- mean as well as median. Westward drift speeds are almost identical to those in section 2.1.

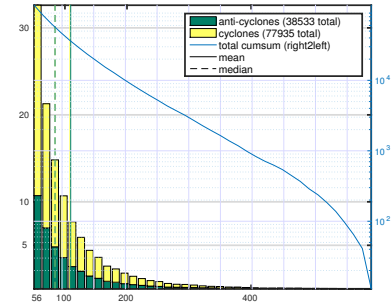


Figure 2.10: Aviso -MII: Final age distribution. x-axis: [days], Left y-axis: [1000]

places of birth and death. size indicates final age.

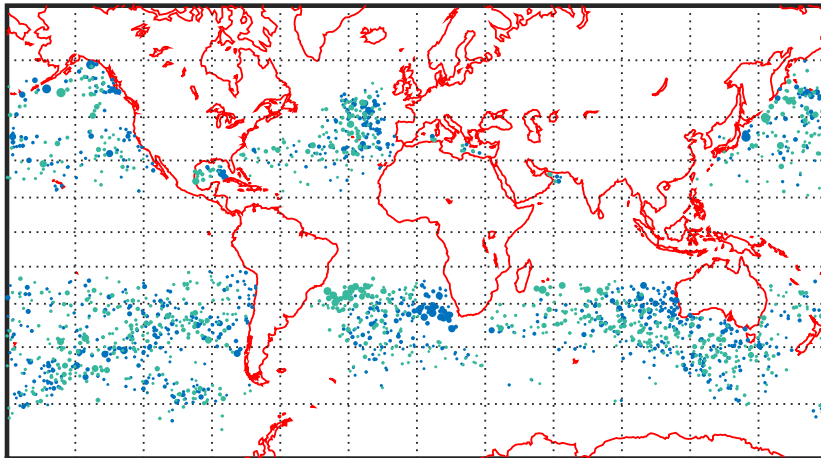


Figure 2.11: Aviso -MII: Births are in blue and deaths in green. Size of dots scales to age squared. Only showing tracks older than one year.

### 2.3 MII - 7 day time-step - POP

THE MODEL DATA delivers slightly more total tracks with a similar 2-fold dominance of cyclones over anti-cyclones (compare figs. 2.10 and 2.15). Similar to Aviso-MII , very long tracks are fewer than via Aviso-MI<sup>4</sup>. The regional pattern looks somewhat similar to the satellite patterns in terms of which regions feature the strongest eddy activity. With the exception of an unrealistic abundance of eddies right along the Antarctic coast where no eddies were detected for the satellite data likely due to sea ice and/or the inherent lack of polar data due to the satellites' orbit-inclinations.

THE more important difference between model- and satellite regional distributions is that the model results indicate significantly less eddy activity away from regions of strong SSH gradients, in the open ocean away from coasts and strong currents. The algorithm also detects hardly any eddy tracks in tropical regions (see ??). This regional heterogeneity in eddy-activity in the model data is also reflected in the distribution of eddy amplitudes (see ??).

THE SCALE  $\sigma$  is generally smaller for the model-data-based analysis

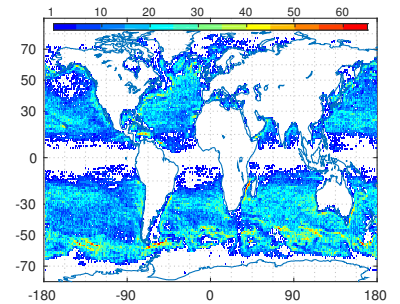


Figure 2.12: Aviso -MII: Total count of individual eddies per degree square. Aviso-MI features 5000 tracks that are older than 400 days, while both MII methods have only  $\sim 1000$  of such.

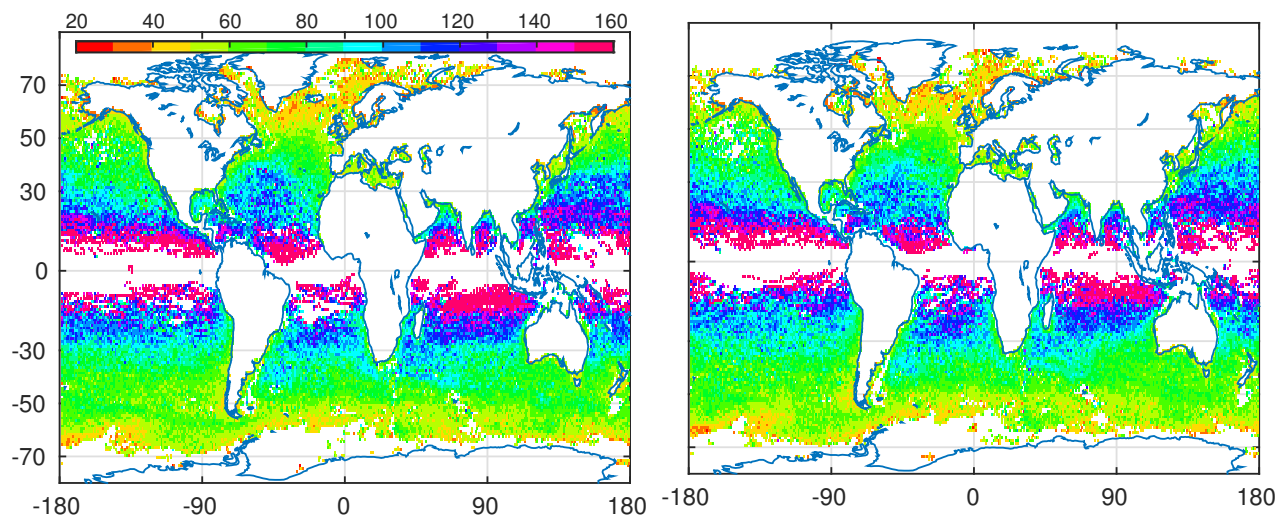
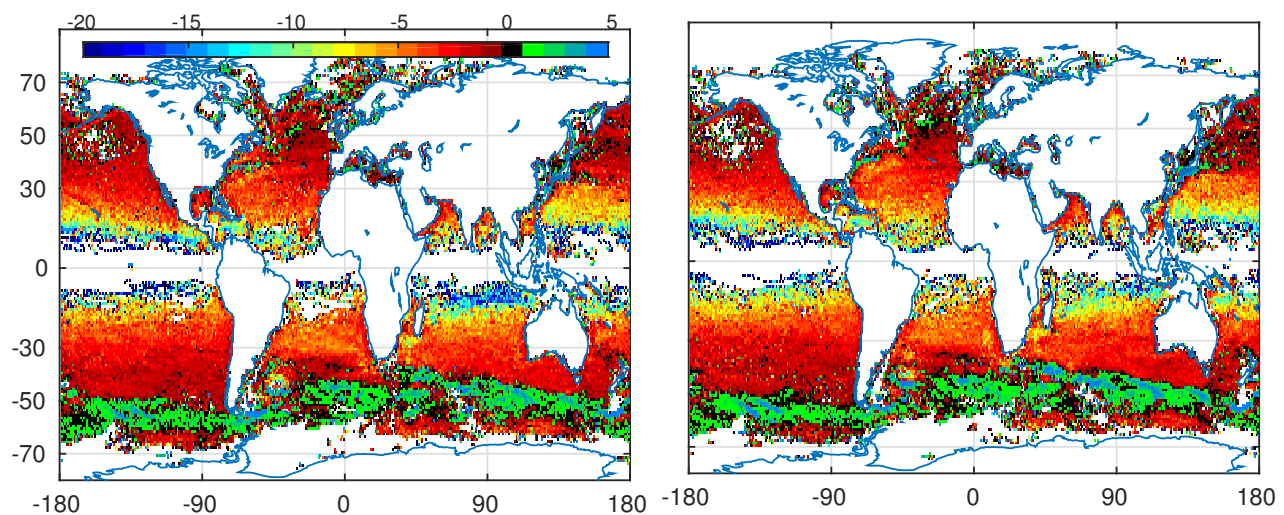
Figure 2.13: Aviso -MII:  $\sigma$  [km]

Figure 2.14: Aviso -MII: zonal translational speed [cm/s]

than for any satellite-based analyses, especially so in high latitudes.

WESTWARD DRIFT SPEEDS look regionally similar to those from satellite data (figs. 2.14 and 2.18). In the zonal mean their magnitude is below those from satellite (see fig. 2.20).

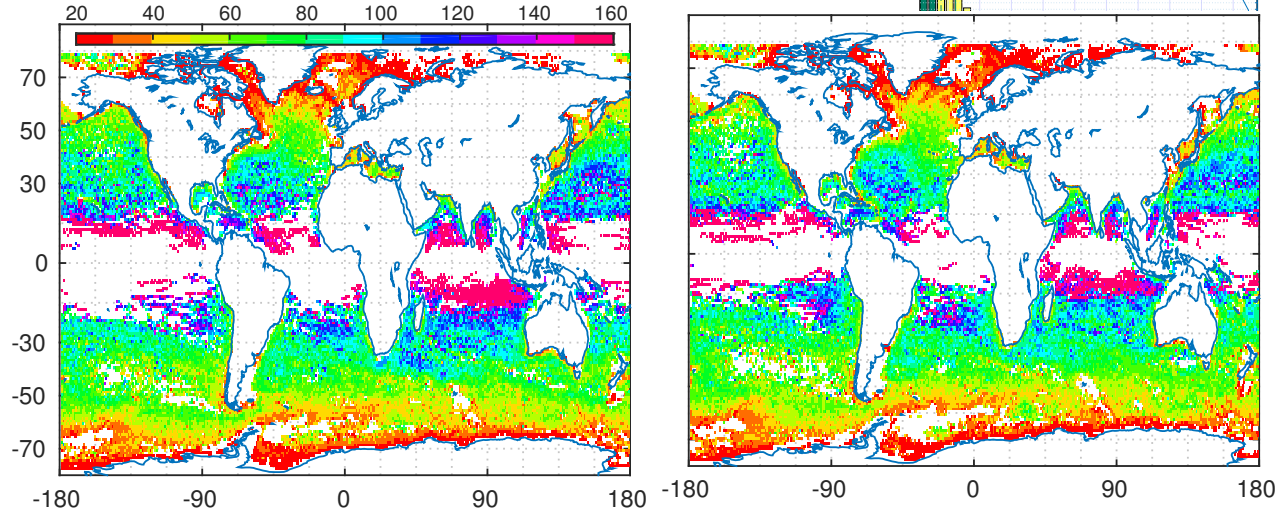


Figure 2.17: pop7-MII:  $\sigma$  [km]

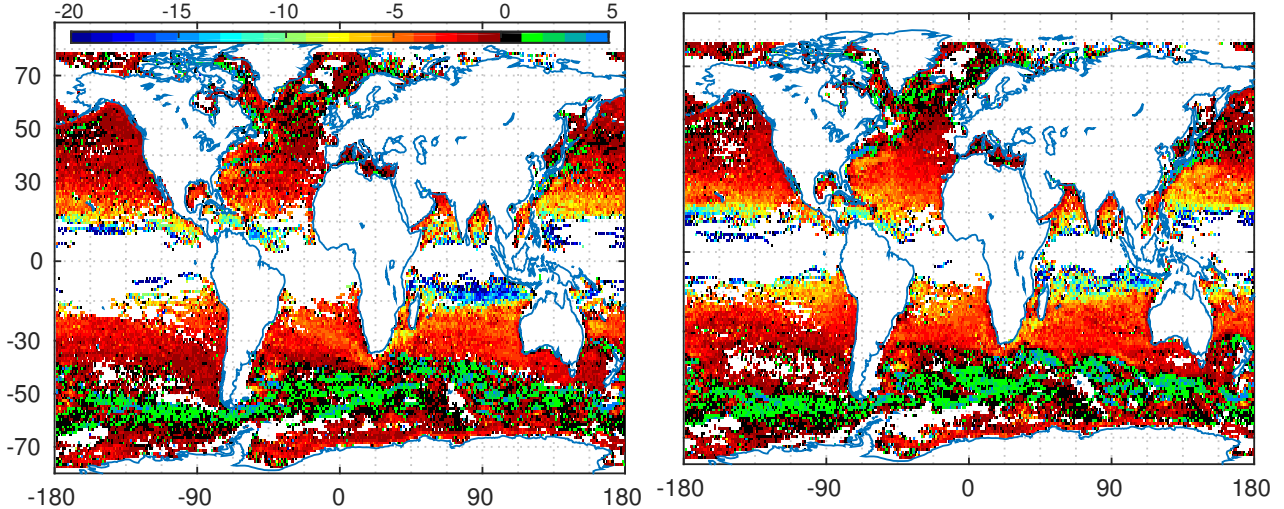


Figure 2.18: pop7-MII: zonal translational speed [cm/s]

## 2.4 MII - 2 day time-step - POP

**TODO:** run is finished. Results will be looked at / interpreted next week

### 2.4.1 **TODO:** net U

**TODO:**

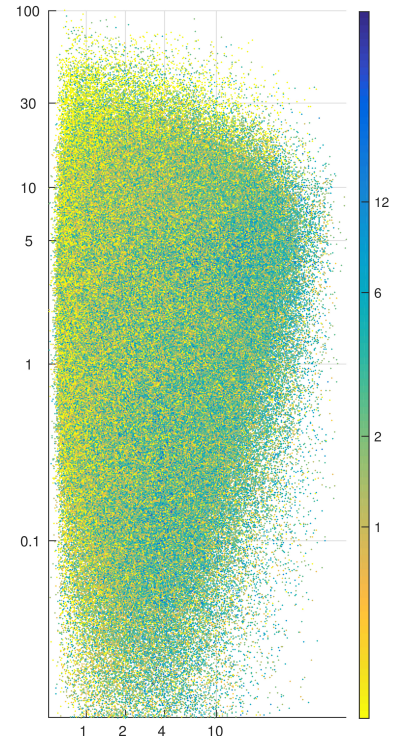


Figure 2.19: pop7-MII: Small amplitude correlates with a short life and a broad translational speed spectrum. y-axis: translational speed [cm/s], x-axis: amplitude [cm], color: age [months].

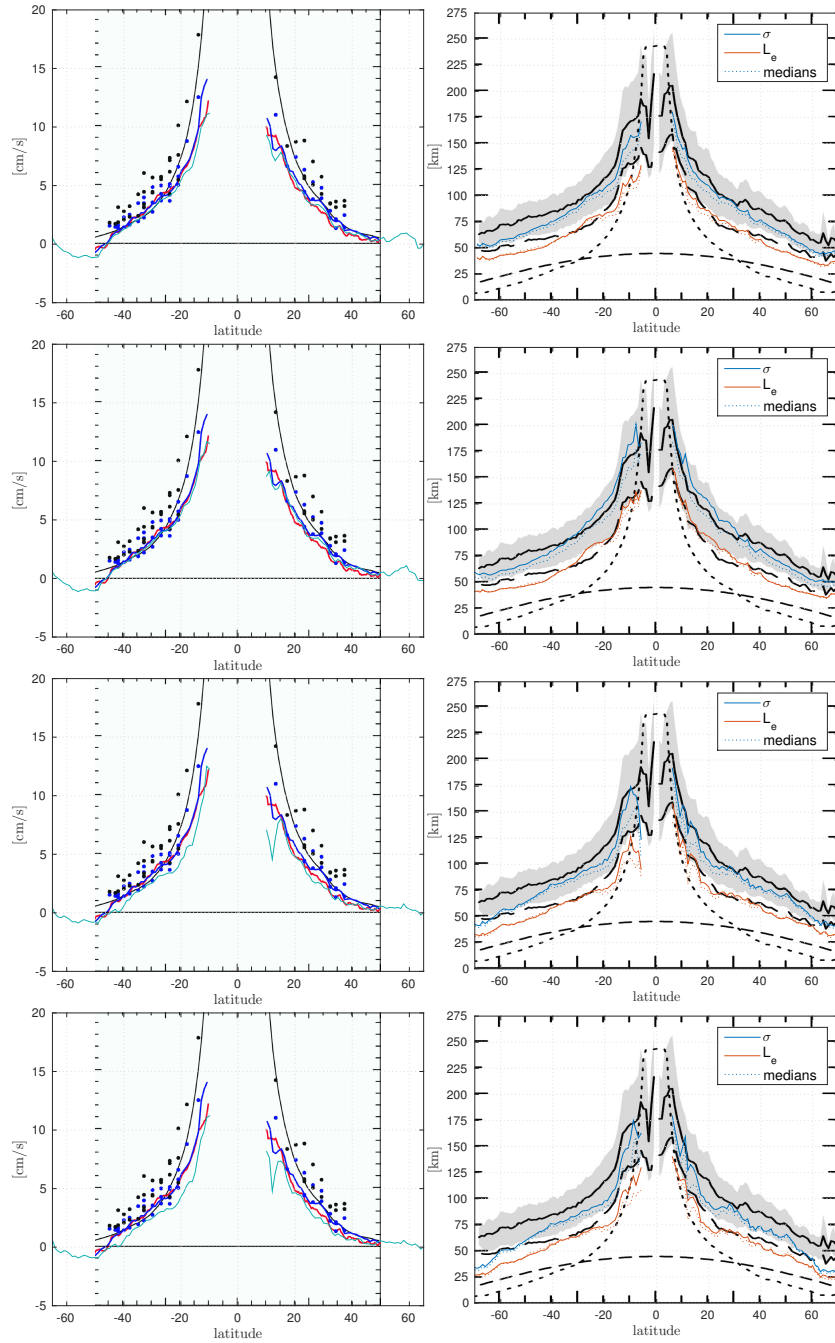


Figure 2.20: Left: Zonal-mean drift speed (cyan) fit to Fig 22 of (?) (Background). Right:  $\sigma$  and  $L_e$  fit to Fig. 12 of their paper. Dotted lines are medians instead of means. 1st row: Aviso-MII , 2nd row: Aviso-MI , 3rd row: pop2avi-MII , 4th row: POP-7day-MII . Note that for the very high latitudes ( $> |60^\circ|$ ) the contrast between model and satellite data is further intensified by the lack of satellite data (see figs. 2.13 and 2.17) in those regions (sea-ice / orbit inclinations). For a depiction without this effect see fig. 3.4. Regarding the underlying figures ? explain: [Left] The black dots are the Radon transforms of the  $20^\circ \times 10^\circ$  high-pass filtered SSH fields along [...] zonal sections [...] The red dots are the average along the propagation speeds of eddies with lifetimes  $> 16$  weeks within  $\pm 1.5^\circ$  of latitude of the center latitudes of the same 45 zonal sections. The latitudinal profile of the global zonal average of the propagation speeds of all of the eddies with lifetimes  $> 16$  weeks is shown by the red line [...]. The black line is the latitudinal profile of the zonally averaged westward phase speeds of long baroclinic Rossby waves. [Right] [...] Meridional profiles of the average (solid line) and the interquartile range of the distribution of  $L_s$  (gray shading) in  $1^\circ$  latitude bins. The long dashed line is the meridional profile of the average of the e-folding scale  $L_e$  of a Gaussian approximation of each eddy [...]. The short dashed line represents the  $0.4^\circ$  feature resolution limitation of the SSH fields of the AVISO Reference Series for the zonal direction [...] and the dotted line is the meridional profile of the average Rossby radius of deformation [...].

# 3

## Discussion

### 3.1 Lengths of Tracks

THE most apparent difference between the results of the [two detection-methods](#) is the abundance of long-lived eddies resulting from the MI-method. This discrepancy must logically be caused by the two different contour-shape testing-procedures (see [box 3](#) and ??), since it is here where the main difference between the two methods' algorithms lies.

THE MI-method is the more lenient one, as all it checks for is whether the contour is of sufficiently compact form. The only shapes that are dismissed are long, thin elongated structures. This means that *e.g.* an eddy track can more easily <sup>1</sup> survive situations in which two eddies merge into one or those in which one is split into two or situations in which mean current gradients distort the vortex (see [fig. 3.2](#)). There could also be the situation in which an old, weak eddy fades, yet another one emerges in sufficient proximity. These two events would not even have to coincide at the exact same time, as long as some short-lived coherent structure, of which there is an abundance <sup>2</sup> at any given time-step throughout the world ocean, acted as a *bridge* to fill the gap.

THE MII-method is conceptually different in that it is based on the assumption that a distinct coherent vortex need *per definition* to be more or less circular. It will therefore be more likely to regard *e.g.* the situation in which one eddy merges with another as a situation of 3 eddies in total; **two** that have just died to create **one** new one. The focus here

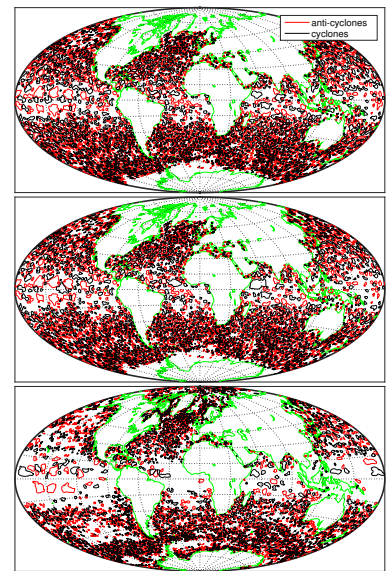


Figure 3.1: All contours that passed the filtering procedure for one exemplary time-step. Top: Aviso-MI . Mid: Aviso-MII . Bottom: POP-7day-MII .

<sup>1</sup> as long as the similarity-criterion is not violated.

<sup>2</sup> see ??

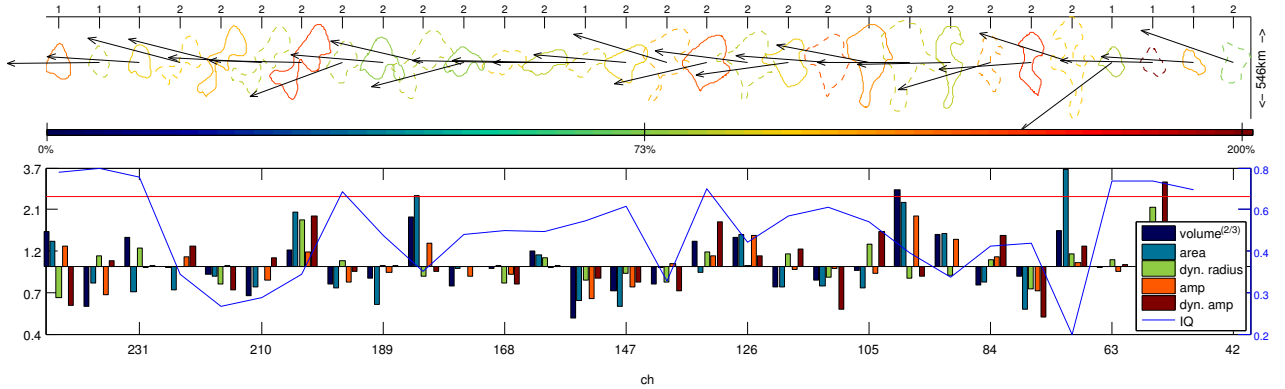


Figure 3.2: The MI-method. Top: Consecutive contours of one track. Colors indicate percentage of change of contour's area with respect to the prior time-step. Topmost horizontal axis shows the (rounded) factor of  $\sigma$  with respect to the local first baroclinic  $L_R^1$ . Vectors' lengths are proportional to the distance travelled with respect to the next time-step. Bottom: Blue graph shows the current IQ. Bars show the factors of change of respective parameters with respect to the prior time-step. X-axis are days since birth.

is more on the propagation of distinct circular geostrophic vortices whereas the focus in the MI-method is more general on coherent local depressions respective elevations in SSH (see fig. 3.3). It should be interesting to look at to which degree tracers found within tracked eddies remaine within the eddy over time (postponed for now). This could further clarify the hypothesis that the MI-method might be better at tracking water-mass advecting entities, with less jumps between bodies of water within one track. E.g. looking at temperature/salt at the eddy's core as a function of time. The downside of the IQ-method is that the identity checks between time-steps fail more easily in the case of merging/splitting situations, thus cutting tracks short. I.e. in the case of one large eddy absorbing another, it does not *die*, but its contour becomes temporarily disfigured and it might thus fail the id check. It comes again down to a question of definition *i.e.* if one large eddy splits into two small ones are we talking about three, or two unique eddies in total?

### 3.2 Scales and the Effect of Downampling

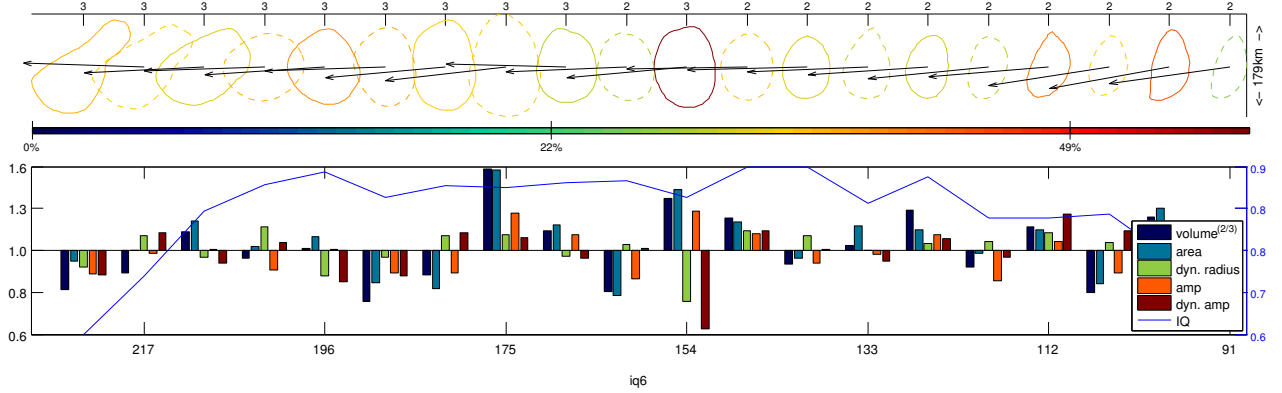


Figure 3.3: The MII-method (IQ-threshold at 0.6). (see fig. 3.2)

INTERESTINGLY , even in the Aviso-MI results, the horizontal eddy scale  $\sigma$  differs from that presented by ?. For latitudes  $\gtrsim |25^\circ|$  the zonal mean here is smaller than theirs while for low latitudes it is higher (see fig. 2.20 and ??). The reason for this discrepancy is suspected to stem from the special method by which  $\sigma$  is determined by our algorithm. As outlined in ??, here  $\sigma$  is half the mean of zonal and meridional distances between the first two local extrema of the first derivative of interpolated 4th-order fourier fits to the SSH data around the eddy's CoV. ? calculate the respective scale via a *direct estimate based on the contour of SSH within the eddy interior around which the average geostrophic speed is maximum*. I.e. they derive  $\sigma$  directly via the area described by the contour of maximum  $|\nabla u|$  and not via any Fourier-type fit.

THE motivation to use fits instead of the SSH directly was on the one hand to avoid noise complicating correct determinations of the 2nd differential zero-crossings and on the other hand to tackle the problem of coarse resolution, especially so for high latitudes where  $\sigma$  seems to become as small as only twice the distance between data points. At this resolution the *Gaussian RMS width* of an eddy would amount to only 5 data points. Since  $\sigma$  is generally smaller in the higher-resolution POP-data analyses, we hypothesize that the scales by ? are biased high for high latitudes. Question remains to what degree this bias is inherent to the Aviso product i.e. as a smearing effect from the interpolation of multiple coarse satellite data. Or

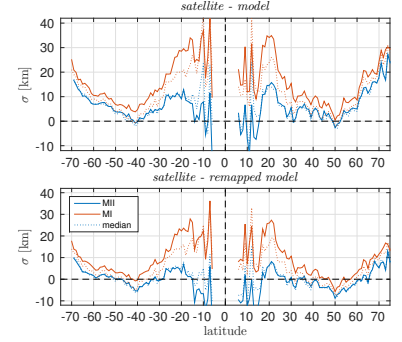


Figure 3.4: Differences in zonal mean  $\sigma$  between Aviso/POP and Aviso/down-sampled POP. Means/Medians are built zonally over only those  $1^\circ \times 1^\circ$ -bins that feature data in both sets i.e. the intersection of  $lat + 1i\ lon$  of both sets.

whether it is attributable entirely to the particular method by which the diameter/area of the zero-vorticity contour is estimated.

STRONG zonal skewness (see ??) suggests the existence of many small, potentially erroneous values that smear the distribution of drift speeds towards an unrealistically low mean. This effect appears to be relevant in e.g. the Southern Ocean, where the east-ward advection of eddies by the ACC results in a broad spectrum of drift speeds. The strong gradients in mean current also effect an abundance of eddy - merging and -splitting situations over relatively short periods of time. It is therefore difficult for the algorithm to keep track of sufficiently long-lived, coherent vortices. Especially so for large time-steps and a high age-threshold. Yet, if the minimum time-step is limited, as in the case of satellite data, a high age-threshold is necessary since short tracks with few data points in time are more likely to stem from erroneously matched contours that do not represent the actual track of a single vortex but instead represent other mesoscale noise that happened to feature sufficiently similar blobs popping in and out of existence at sufficient proximity to one another.

WITH REGARD to the lower latitudes two important aspects need to be considered:

1. The analyses yield generally low eddy activity in the tropics. Hence the results are less robust in this region *a priori*.
2. The standard deviation in  $\sigma$  is particularly broad in the tropics (see fig. 3.5). As a matter of fact it appears as though there might be two different types of eddies. One type analogous to all high-latitude eddies and a new one of much larger scale. Because these larger eddies have generally low IQ-values they are filtered from the MII analyses, resulting in smaller tropical  $\sigma$ . Their more chaotic shape might, due to the different methods to determine  $\sigma$ , also have to do with why mean tropical  $\sigma$  is larger here than in ?.

THE POP-7day-MII analysis yields somewhat similar  $\sigma$  for low latitudes <sup>3</sup>, yet significantly smaller values for high latitudes. The

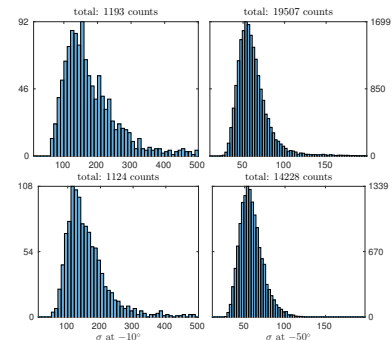


Figure 3.5: Eddy count at one point in time for one fully zonal  $1^\circ$ -bin. Top: Aviso-MI . Bottom: Aviso-MII . The tropical spectrum is broad yet with strong positive skewness *i.e.* oriented towards smaller scales. In high latitudes the standard deviation is smaller. The MI method yields more large eddies.

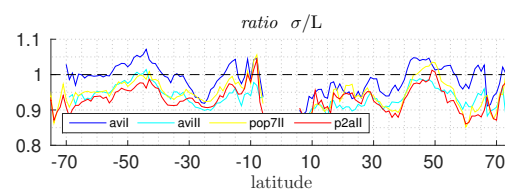


Figure 3.6: Ratios of  $\sigma$  to  $L$  (see ??). In the ideal case of a perfect Gaussian profile,  $\sigma$  and  $L$  would be equivalent. **TODO: take out? Dont make no sense**

<sup>3</sup> Note that due to the lack of tropical eddies the estimates of  $\sigma$  are rather uncertain for the POP analyses.

question here therefor is whether this discrepancy is a result of the lower resolution of the satellite data *i.e.* that eddies are too small to be resolved by the Aviso product in high latitudes or whether it is attributable to the model data as in a systematic bias due to incomplete/poorly parameterized model physics. This question was the primary motivation for the pop2avi-MII -run. The idea here was to down-size the POP data to the geometry of the Aviso grid in order to test whether this would raise  $\sigma$  to that from the satellite results. Figure 3.4 shows that the down-sampling did indeed decrease the discrepancy in  $\sigma$  to respective Aviso analysis, as long as those regions that are unique to either data set are excluded. Between  $\pm 25^\circ$  and  $\pm 65^\circ$  the difference is no larger than  $\pm 5$  km. This came as a surprise because since  $\sigma$  stems from Fourier fits of SSH, we expected the original frequencies to be, at least to some extent, conserved in the down-sampled data.

### 3.3 Drift Speeds

ZONAL mean drift speeds of all Aviso results agree well with those presented by ? (see fig. 2.20), suggesting that the tracking procedures are relatively robust for both the MI and MII methods.

THE POP-7day-MII results yield generally smaller magnitudes of  $u$ . The apparent drop in magnitude at  $\sim 12^\circ\text{N}$  is most likely due to erroneous inter-time-step eddy-associations (fig. 2.20). In that region, the combination of extreme sparsity of results, large time-step, large  $\sigma$ , low amplitude and high (theoretical) drift speed make robust determinations of  $u$  practically impossible. Yet the tendency for lower magnitudes in  $u$ , albeit less stark, is also true for higher latitudes. The zonal drift speeds are calculated via gradients of *polyfits* to the CoV-locations on the surface of a spherical earth. This method was tested thoroughly and its robustness is further validated by the fact that the weaker  $u$  remains approximately the same after down-sampling for the pop2avi-MII run. Yearly sub-samples of the zonal-mean profiles <sup>4</sup> further prove the consistency of the drift-speeds over time for both data.

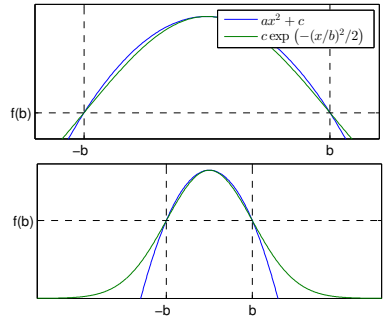


Figure 3.7: The upper part of a Gaussian profile can appear similar to a quadratic one. **TODO:** ref to here

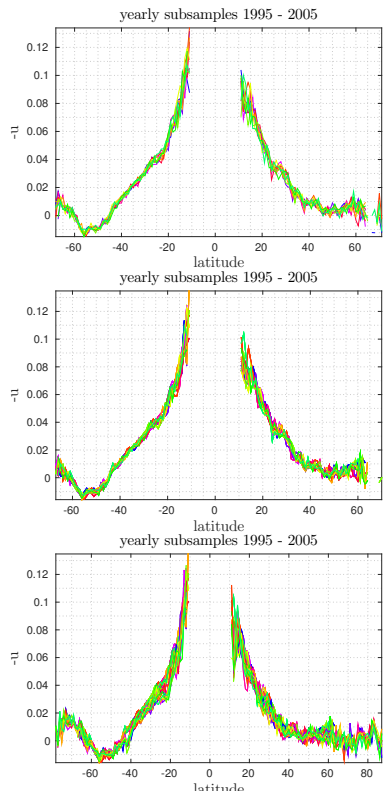
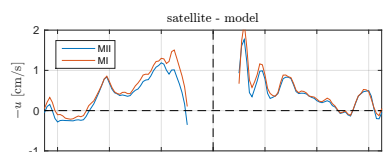


Figure 3.8: Each line represents zonal means of tracks that ended within one of the eleven years from 1995 to 2005. Top: Aviso-MI . Middle: Aviso-MII . Bottom: POP-7day-MII .

<sup>4</sup> see section 3.3



FROM equation (1.5) we know that at first approximation (planetary lift)

$$u \sim \beta \left( \frac{NH}{f} \right)^2 \quad (3.1)$$

Since  $\beta, H$  and  $f$  should have been set realistically in POP, it appears that the, evidently unrealistic, drift speeds in the model results stem from an unrealistic or poorly resolved (only 42 vertical layers in POP) density stratification  $\frac{\partial \rho}{\partial z}$ .

A general problem with the depiction of drift-speeds as zonal means is that  $u$ , besides latitude, is also strongly dependent on longitude.

Figures 2.12 and 2.16 show strong regional heterogeneity of  $u$  presumably influenced by  $f/H$ -contours, density stratification and mean flow ???. Note, for example, how the area at  $15^{\circ}\text{S}$  west of Australia shows regional drift speeds of  $> -15 \text{ cm/s}$  whilst the zonal mean of  $u$  amounts to only  $\approx -6 \text{ cm/s}$ . It appears that generally areas of strong eddy-activity yield larger values for  $u$  than do areas of weaker meso-scale dynamics (see also figs. 2.19 and 3.10 and ??).

### 3.4 POP-2day-MII

So far, all analyses used a 7 d-time-step. As already mentioned in section 1.3, from the results we know that eddies translate at speeds on the order  $\mathcal{O}(10^0) \text{ cm s}^{-1}$  to  $\mathcal{O}(10^1) \text{ cm s}^{-1}$  or up to  $100 \text{ km/7 d}$  and apparently even more in low latitudes. This means that one eddy's location might well change as much as its own scale and more over one time-step. Taken how tightly packed eddies often are in areas of high activity, *i.e.* directly adjacent to one another akin to an egg's box (see *e.g.* section 3.1), raises the issue whether the weekly resolution in time is sufficiently fine to successfully track individual eddies and thus deliver realistic translative-speed statistics. In order to investigate the influence of a shorter time-step the POP-7day-MII - run was repeated, only this time with a 2 d time-step.

The effect is only small in the zonal mean (see fig. 3.11). But regionally some noteworthy differences to the weekly analysis emerge (see fig. 3.12):

- Westward drifts are now faster in low latitudes, suggesting that the 7-day time-step is in deed too large to correctly associate all of the large, fast tropical eddies.

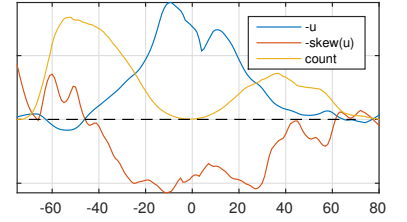


Figure 3.10: Skewness (red) of  $-u$  for Aviso-MI. The spectrum leans towards high westward values in low latitudes. In the ACC the distribution reverses, indicating the existence of sporadic (in time or space (x-dir.)) events of strong eastward advection by the mean flow. (Note: Everything normalized to fit all in one frame.)

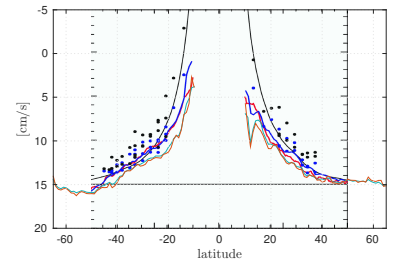


Figure 3.11: Same plot as the one POP-7day-MII one from fig. 2.20 with the result from POP-2day-MII added in brown.

- Areas of strong drift-speed gradients as along the western boundary currents and the ACC show slight general disagreement between the two analyses, suggesting that the the analyses benefits from more available time-frames.

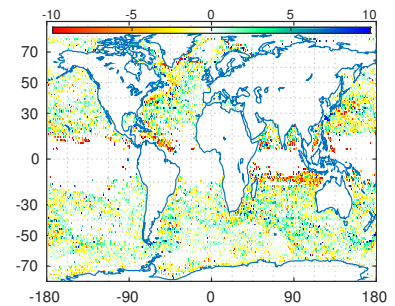


Figure 3.12: Zonal drift speed of POP-2day-MII minus POP-7day-MII [ $\text{cm s}^{-1}$ ].



## *Declaration of Authorship*

I, Nikolaus KOOPMANN, declare that this thesis titled, *A Global Analysis of Mesoscale Eddy Dynamics via a Surface-Signature-Based Tracking Algorithm* and the work presented in it are my own. I confirm that:

- Where I have consulted the published work of others, this is always clearly attributed.
- Where I have quoted from the work of others, the source is always given. With the exception of such quotations, this thesis is entirely my own work.
- I have not submitted the work to any other examination procedure.
- The submitted printed version is the same as the submitted digital version.

Signed: \_\_\_\_\_

Date: \_\_\_\_\_



## *Declaration of Authorship*

Ich, Nikolaus KOOPMANN, versichere an Eides Statt durch meine Unterschrift, dass ich die vorstehende Arbeit mit dem Titel *A Global Analysis of Mesoscale Eddy Dynamics via a Surface-Signature-Based Tracking Algorithm*, :

- selbständig und ohne fremde Hilfe angefertigt und alle Stellen, die ich wörtlich oder dem Sinne nach aus Veröffentlichungen entnommen habe, als solche kenntlich gemacht habe, mich auch keiner anderen als der angegebenen Literatur oder sonstiger Hilfsmittel - insbesondere keiner im Quellenverzeichnis nicht genannten Internetquellen - bedient habe.
- ich die Arbeit vorher nicht in einem anderen Prüfungsverfahren eingereicht habe.
- die eingereichte schriftliche Fassung der auf dem elektronischen Speichermedium entspricht.

Unterschrift:

Datum:

**TODO: bibtex warnings**

**TODO: abc**

**TODO: check overlaps of figs**

**TODO: abstract**